*Annals of Biomedical Engineering*, Vol. 31, pp. 284–293, 2003
Printed in the USA. All rights reserved.

0090-6964/2003/31(3)/284/10/$20.00


# A Model for Transport and Dispersion in the Circulatory System Based on the Vascular Fractal Tree

ARISTIDES DOKOUMETZIDIS and PANOS MACHERAS

School of Pharmacy, University of Athens, Panepistimiopolis, 157 71 Athens, Greece

*(Received 14 March 2002; accepted 19 December 2002)*

**Abstract—**Materials are distributed throughout the body of mammals by fractal networks of branching tubes. Based on the scaling laws of the fractal structure, the vascular tree is reduced to an equivalent one-dimensional, tube model. A dispersion–convection partial differential equation with constant coefficients describes the heterogeneous concentration profile of an intravascular tracer in the vascular tree. A simple model for the mammalian circulatory system is built in entirely physiological terms consisting of a ring shaped, one-dimensional tube which corresponds to the arterial, venular, and pulmonary trees, successively. The model incorporates the blood flow heterogeneity of the mammalian circulatory system. Model predictions are fitted to published concentration-time data of indocyanine green injected in humans and dogs. Close agreement was found with parameter values within the expected physiological range. © *2003 Biomedical Engineering Society.*
[DOI: 10.1114/1.1555627]

**Keywords—**Fractal tree, Indocyanine green, Tracer kinetics, Dispersion, Tube.

## INTRODUCTION

The branching pattern of the vascular system and the blood flow through it has continued to be of interest to anatomists, physiologists, and theoreticians.[2,5,8] The studies focusing on the geometric properties such as lengths, diameters, generations, orders of branches in the pulmonary, venular, and arterial tree of mammals uncovered the principles on which these properties are based. Vascular trees seem to display roughly the same dichotomous branching pattern at different levels of scale, a property found in fractal structures.[12,17,30,35] The hydrodynamics of blood flow in individual parts of the dichotomous branching network, has been the subject of various studies since the flow changes from pulse-wave flow in major vessels to Poiseuille-type flow in small vessels.[7,14,16,20,27,34] Recently, West *et al.*,[32] relying on an elegant combination of the dynamics of energy transport and the mathematics of fractal geometry developed a hydrodynamic model that describes how essential materials are transported through space-filling fractal networks of branching tubes. The major contribution of the West *et al.*[32] model is the interpretation of the origin of allometric laws in biology and the finding that the internal structure of living things operates as if they were four-dimensional.[33]

Although these advances of science[32,33] provide an analysis of the scaling relations for mammalian circulatory systems, models that describe the transport of materials along the entire fractal network of the mammalian species are needed, too. Pharmacokinetics and toxicokinetics which are the fields of science that this kind of modeling is of the greatest importance are dominated by the concept of homogenous compartments.[29] Physiologically based pharmacokinetic models have been also developed that define the disposition patterns in terms of physiological principles.[9,29,31] The development of models that study the heterogeneity of the flow and the materials distribution inside vascular networks and individual organs has also been fruitful in the past years.[3,19,23,28] In this work, we develop a simple model for the heterogeneous transport of materials in the circulatory system of mammals, based on a single tube dispersion–convection system which is equivalent to the fractal network of the branching tubes.

## TRANSPORT AND DISPERSION IN THE VASCULAR TREE

### *Geometrical Considerations*

We consider a fractal arterial tree that consists of $N$ branching levels where each level consists of parallel vessels, Fig. 1(A). Each vessel is connected to $n$ vessels of the consequent branching level.[32] The vessels are nonelastic tubes, inside which incompressible fluid flows. Nonlinearities at the junctions of the vessels are ignored. We make the assumption that the vessel lengths in each level $k$ follow a distribution around the mean value $l_k$. The total flow across a section of the entire tree is constant (conservation of mass). This allows us to replace the tree with a single one-dimensional tube, an idea that

Address correspondence to Panos Macheras, School of Pharmacy, University of Athens, Panepistimiopolis, 157 71 Athens, Greece. Electronic mail: macheras@pharm.uoa.gr

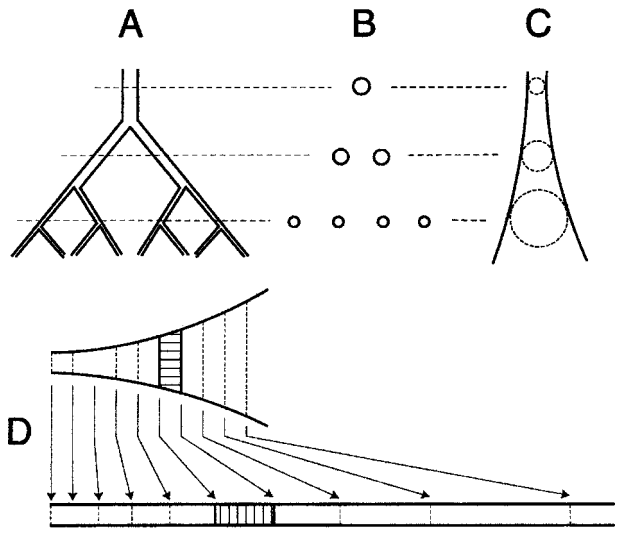


**FIGURE 1. (A) Schematic representation of a dichotomous branching network. (B) Cross sections at each level. (C) Tree is replaced by a single tube with continuously increasing radius. The area of the cross section of the tube is equal to the total area of the cross sections of each level of the tree. (D) Volume preserving transformation of the varying radius tube (C) to a fixed radius tube.**

has been applied before for the transport of gas in the pulmonary airways.[24] Since the tree is not area preserving, the total cross section area of subsequent levels increases, i.e., the tube is not cylindrical [Figs. 1(A)–1(C)]. However, an appropriate geometrical transformation can be used to replace the noncylindrical tube with a simple cylinder [Fig. 1(D)]. Thus, the fluid velocity remains constant throughout the tube in consequence of this transformation.

The derivation of the geometrical transformation is based on the scaling properties of the fractal tree. The noncylindrical tube is described in terms of a continuous spatial coordinate, $x$, which replaces the $N$ branching levels of the fractal tree from the aorta to the capillaries. Let level 0 be the top vessel of the tree. The area of the cross section at the beginning of the tube is $A_0=\pi r_0^2$, where $r_0$ is the radius of the top vessel (the aorta for the arterial tree). The total cross section at level $k$ of the tree is $A_k=\pi r_k^2 N_k$, where $r_k$ is the radius of the vessel at level $k$ and $N_k=n^k$ is the number of vessels.[32] In reality the radii at each level $k$, are distributed around the mean value $r_k$. The variance of the radii distribution produces the heterogeneity of the velocities. The radii scale according to the ''cubic law'' branching, $\beta=n^{-1/3}$, where $\beta=r_{k+1}/r_k$. These relations give $r_k=r_0\beta^k$ leading to $A_k=\pi r_0^2 n^{k/3}$. In the same rationale with the radii,[32] we have for the mean value of the vessel lengths $l_{k+1}/l_k=\gamma=n^{-1/3}$ and so the length of the vessel at level $k$ is $l_k=l_0\gamma^k$. The mean value of the total length, $l_k$, of a path from the top of the tree to the beginning of the level $k$, is the value of $x$ coordinate,

$$x\equiv L_k=\sum_{i=0}^{k-1}\gamma^i l_0=\sum_{i=0}^{k-1}n^{-i/3}l_0=\frac{n^{1/3}-n^{(1-k)/3}}{n^{1/3}-1}l_0. \quad (1)$$

Solving the last expression for $k$ yields

$$k(x)=1+\frac{3\ln l_0-3\ln(x-xn^{1/3}+l_0n^{1/3})}{\ln n}. \quad (2)$$

Substituting Eq. (2) in the expression of $A_k$, we have

$$A(x)\equiv A_k=\frac{\pi r_0^2 l_0 n^{1/3}}{x-xn^{1/3}+l_0n^{1/3}}. \quad (3)$$

The last expression gives the area $A(x)$ of the noncylindrical tube, Fig. 1(C), as a function of the coordinate $x$. Further, a volume preserving transformation allows the replacement of the varying radius tube with a tube of fixed radius $r_0$, the radius of the aorta [Fig. 1(D)]. This is accomplished by replacing $x$ with a new coordinate $x'$ with the condition that the constant total flow of the fluid, $J=dV/dt$, across a section is kept invariant under the transformation. Accordingly, the corresponding area $A'(x')$ is $\pi r_0^2$ for every $x'$; thus, $Jdt=dV=A(x)dx=A'(x')dx'$. Integrating, we have $\int_0^{x'}A'(x')dx'=\int_0^x A(x)dx$. Using Eq. (3) for $A(x)$ and calculating the integral, we finally get the exact formula of the transformation,

$$x'=\frac{l_0n^{1/3}}{n^{1/3}-1}\ln\left(\frac{l_0n^{1/3}}{x-xn^{1/3}+l_0n^{1/3}}\right). \quad (4)$$

Also, solving Eq. (4) for $x$, the inverse transformation can be obtained,

$$x=\frac{l_0n^{1/3}}{n^{1/3}-1}\left(1-\exp\frac{x'(1-n^{1/3})}{l_0n^{1/3}}\right). \quad (5)$$

Inspection of Eq. (4) reveals that the new coordinate system is a kind of ''logarithmic scale.'' A consequence of the transformation is that if we go back to the discrete levels, the length of each level in the new coordinate system is the same for all $k$, namely,

$$l_k'=x'(k+1)-x'(k)=\frac{\ln n}{3\tilde{n}}l_0, \quad (6)$$

where $\tilde{n}=1-n^{-1/3}$, which is independent of $k$.

It should be noted that according to West *et al.*,[32] the larger vessels (aorta and major arteries) have area preserving branching. This portion of the tree can be integrated in our model easily by adding an initial cylindrical segment in the tube model [Fig. 1(D)]. This segment does not require any transformation, since both the radius of the cylindrical segment and the velocity of the fluid in it are constant. Since this cylindrical segment does not alter the dynamics of the model considerably, it was left out for simplicity.

### *Solute Kinetics*

The disposition of a solute in the fluid as it flows through the system is governed by convection and dispersion. The convection takes place with velocity

$$u(x)=\frac{\pi r_0^2}{A(x)}u_0=\frac{x-xn^{1/3}+l_0n^{1/3}}{l_0n^{1/3}}u_0. \tag{7}$$

The dispersion consists of three components. The molecular diffusion which is considered negligible. The geometrical dispersion which originates from the variance of the path lengths as the blood flows through progressively smaller vessels, and the geometrical dispersion which originates from the variance of the velocities. The latter is due to the variance of the vessel radii. Thus, the dispersion coefficient, $D(x)$, is of the form

$$D(x)=D_l(x)+D_r(x), \tag{8}$$

because the two components are independent from each other. The first term $D_l(x)$ is proportional to the velocity, $u(x)$,[6] and the variance of the path lengths, $\sigma_l(x)$, of the same branching level, thus,

$$D_l(x)=a_1.\sigma_l(x)u(x). \tag{9}$$

Although it is reasonable to assume a nonsymmetrical distribution of the vessel length such as lognormal, in most morphometric studies the measure of the spread around the mean value is reported as a standard deviation value.[3] The functional form of $\sigma_l(x)$ as blood goes down the branching levels is given by a power law, similar to the one of the lengths and the radii, namely, $\sigma_k=\sigma_{l0}\delta^k$.[13] It should be noted that $\sigma_{l0}$ is a proportionality constant and does not stand for the variance at level 0, as this level has only one vessel and thus the variance is zero. The exponential law for $\sigma_k$ is in accordance with morphometric data of pulmonary vasculature[13] for the level 1 and on, but since this model engages continuous geometry the relation is used for all levels. The morphometric data of the branching pattern and vascular geometry, also suggest that $\delta=\gamma=n^{-1/3}$; this is so since $\sigma_k/l_k$ is almost constant for all $k$.[13] Hence, $\sigma_l(x)$ can be expressed using Eqs. (2) and (3):

$$\sigma_l(x)=\sigma_{l0}\delta^{k(x)}=\sigma_{l0}n^{-k(x)/3}=\frac{x-xn^{1/3}+l_0n^{1/3}}{l_0n^{1/3}}\sigma_{l0}$$
$$=\frac{\pi r_0^2}{A(x)}\sigma_{l0}. \tag{10}$$

So,

$$D_l(x)=a_1\left(\frac{\pi r_0^2}{A(x)}\right)^2\sigma_{l0}u_0. \tag{11}$$

The second term $D_r(x)$ of Eq. (8), as already mentioned originates from the variance of the velocities as a result of the variance of the radii:

$$D_r(x)=a_2\sigma_u(x)l(x). \tag{12}$$

The velocity as a function of the radius is

$$u(x)=\frac{r_0^2}{N(x)r^2(x)}u_0. \tag{13}$$

So the variance of $u(x)$ as a function of the variance $r(x)$ can be derived from error propagation theory

$$\sigma_u(x)=2\frac{u(x)}{r(x)}\sigma_r(x), \tag{14}$$

since $u(x)=\pi r_0^2/A(x)\,u_0$ and $r(x)=\pi r_0^2/A(x)\,r_0$, we have

$$\sigma_u(x)=2\frac{u_0}{r_0}\sigma_r(x). \tag{15}$$

In the same manner as with the variance of the lengths, it is reasonable to assume that the variance of the radii of the same level is of the form $\sigma_r(x)=[\pi r_0^2/A(x)]\,\sigma_{r0}$. This is justified by the morphometric data of the pulmonary vasculature;[13] however, the values of the radii variance seem to be rather small compared to the respective values of the lengths. This is probably due to the fact that the Strahler classification system that is commonly used is in fact diameter defined, so one expects that the variance of this parameter to be small.[13]

Also, it holds that

$$l(x)=\frac{\pi r_0^2}{A(x)}l_0. \tag{16}$$

Thus, Eq. (12) can be written

$$D_r(x)=2a_2\left(\frac{\pi r_0^2}{A(x)}\right)^2\frac{\sigma_{r0}l_0u_0}{r_0}. \tag{17}$$

The final form of the dispersion coefficient is obtained by substituting Eqs. (11) and (17) in Eq. (8):

$$D(x)=\left(a_1\sigma_{l0}+2\frac{a_2\sigma_{r0}l_0}{r_0}\right)\left(\frac{\pi r_0^2}{A(x)}\right)^2u_0. \tag{18}$$

The equation which describes the concentration $C$ of a solute inside the tube, is a dispersion–convection partial differential equation (PDE),

$$\frac{\partial C(x,t)}{\partial t}=\frac{\partial}{\partial x}\left(D(x)\frac{\partial C(x,t)}{\partial x}\right)-u(x)\frac{\partial C(x,t)}{\partial x}. \tag{19}$$

Since $u(x)$ depends on $x$ one would feel that a term $-[\partial u(x)/\partial x]C(x,t)$ should also be present in Eq. (19), in order for the mass to be preserved. However, since the cross section of the tube is not constant, the mass is actually preserved.

Applying the transformation $x'=x'(x)$, Eq. (19) becomes

$$\frac{\partial C(x',t)}{\partial t}=D(x)\left(\frac{\partial x'}{\partial x}\right)^2\frac{\partial^2C(x',t)}{\partial x'^2}-\left(-\frac{\partial D(x)}{\partial x}\frac{\partial x'}{\partial x}-D(x)\frac{\partial^2x'}{\partial x^2}+u(x)\frac{\partial x'}{\partial x}\right)\frac{\partial C(x',t)}{\partial x'}. \tag{20}$$

After some algebra (see the Appendix), the equation describing the concentration of the solute, $C(x',t)$, ends up to be a simple convection–dispersion equation with constant coefficients

$$\frac{\partial C(x',t)}{\partial t}=\left(a_1\sigma_{l0}+2\frac{a_2\sigma_{r0}l_0}{r_0}\right)u_0\frac{\partial^2C(x',t)}{\partial x'^2}-\left\{\frac{\tilde{n}}{l_0}\left(a_1\sigma_{l0}+2\frac{a_2\sigma_{r0}l_0}{r_0}\right)+1\right\}u_0\frac{\partial C(x',t)}{\partial x'}. \tag{21}$$

Finally, we can write

$$\frac{\partial C(x',t)}{\partial t}=D_0\frac{\partial^2C(x',t)}{\partial x'^2}-U_0\frac{\partial C(x',t)}{\partial x'}, \tag{22}$$

where

$$D_0=a\cdot u_0 \quad \text{and} \quad U_0=\left(\frac{\tilde{n}}{l_0}a+1\right)u_0,$$

where

$$a=a_1\sigma_{l0}+2\frac{a_2\sigma_{r0}l_0}{r_0}. \tag{23}$$

*Tracer Washout Curve from a Tree-Like Network*

We derived a simple equation [Eq. (22)] to describe the concentration $C$ of a solute in a tree-like structure that corresponds to the arterial tree of a mammal. Considering also the corresponding venular tree situated next to the arterial tree and appropriate inflow and outflow boundary conditions we are able to derive an expression for the spatiotemporal distribution of a tracer inside a tree-like transport network. In order to present an analytical explicit solution we make the assumption that the arterial and venular trees are symmetrical, that is, have the same volume. The boundary conditions that we use are:

Inflow at $x=0$:

$$\left(-D_0\frac{\partial C}{\partial x}+U_0C\right)\Big|_{x=0}=\frac{L}{V}Q(0)\,\delta(t), \tag{24}$$

where $Q(0)$ is the dose, $V$ is the volume of the system, and $\delta(t)$ is the Dirac delta function.

Outflow at $x=L$:

$$\frac{\partial C}{\partial x}\Big|_{x=L}=0, \tag{25}$$

where $L=V/A$ and $A$ is the cross-section area of the inflow (and outflow since the trees are symmetrical). The above boundary conditions indicate that at the inflow and outflow points convection dominates over dispersion. In chemical engineering literature this feature is considered a good choice when the dispersion comes from molecular diffusion. In the case of geometrical dispersion in porous media other boundary conditions that extend the dispersion up to the edges, are considered preferable.[26] However, the inflow and outflow ways consist of single vessels, justifying that convection dominates over dispersion. The outflow concentration $C(L,t)$ of the above system, with initial condition $C(x,0)=0$, is[21]

$$C(L,t)=\frac{Q(0)}{V}e^{U_0L/D_0}\left[\frac{2L}{\sqrt{\pi D_0 t}}\left(1+\frac{U_0^2}{2D_0}t\right)\right.$$
$$\times e^{-(L+U_0t)^2/4D_0t}-\frac{U_0L}{2D_0}\left(4+\frac{U_0L}{D_0}+\frac{U_0^2}{D_0}t\right)$$
$$\left.\times\operatorname{erfc}\left(\frac{L+U_0t}{2\sqrt{D_0t}}\right)\right]. \quad (26)$$

Equation (26) can be fitted straightforward to tracer washout curves from organs that have a tree-like network structure.

## MODEL FOR THE CIRCULATORY SYSTEM

Based on the results of the previous paragraphs we will construct an elementary pharmacokinetic model considering the entire circulatory system. Thus, apart from the arterial and venular trees, a second set of arterial and venular trees, corresponding to the pulmonary vasculature, must be considered as well. These trees follow the same principles based on Eqs. (4) and (22), i.e., tubes of radius $r_0$ are considered with appropriate length to accommodate the correct blood volume in each tree. Thus, an overall tube of appropriate length, $L$, is considered and is divided into four sequential parts, characterized as arterial, venular, pulmonary arterial and pulmonary venular, respectively. The length, $L$, accommodates the total blood volume, $V_b=\pi r_0^2 L$. We assign[10] the first portion of the tube length from $x'=0$ to $x'=x'_c$, to the arterial tree, the next portion from $x'=x'_c$ to $x'=x'_p$ to the venular, and the rest from $x'=x'_p$ to $x'=L$ to the two symmetrical trees of the lungs. We consider that the venular tree is a structure similar to the arterial tree, only of greater, but fixed, capacity. In reality, the venular tree has a variable capacity and acts as a blood reservoir which delivers blood to the tissues additional to the cardiac output.[10] This property of the venular tree is ignored in this model. In the final model the value of the dispersion coefficient takes three separate values introducing discontinuities. We use two separate values for the dispersion coefficient, $D_a$ for arterial segment and $D_p$ for the pulmonary segment. For the venular segment we consider that the dispersion coefficient has the value $D_a(x'_p-x'_c)/x'_c$, which means that it is proportional to the length of the segment. This is because we may also assume that the ratio $\sigma_{r0}/r_0$ is constant for the arterial and venular trees and thus in Eq. (23), $D_0\propto\sigma_{l0}\propto l_0\propto L$. Also, the two ends of the tube are connected, to allow recirculation of the fluid. This is implemented by introducing a boundary condition, namely $C(0,t)=C(L,t)$, which makes the tube ring shaped (Fig. 2). The flux preservation boundary condition, $D_a\,\partial C/\partial x'\,|_0 = D_p\,\partial C/\partial x'\,|_L$, must be also satisfied. The ''heart'' is located at two separate points. The left ventricle-left atrium is situated at $x'=0$ between the arterial and the pulmonary venular segments, while the right ventricle–right atrium is situated at $x'=x'_p$ between the venular and the pulmonary arterial segments. Further, the necessary initial condition for the intravenous administration of an exogenous substance, $C(x',0)$, which is the spatial profile of $C$ at the time of administration, is determined by the initial dose and the type of administration. This profile may have the shape of a ''thin'' Gaussian function, if an intravenous bolus administration is considered, namely,

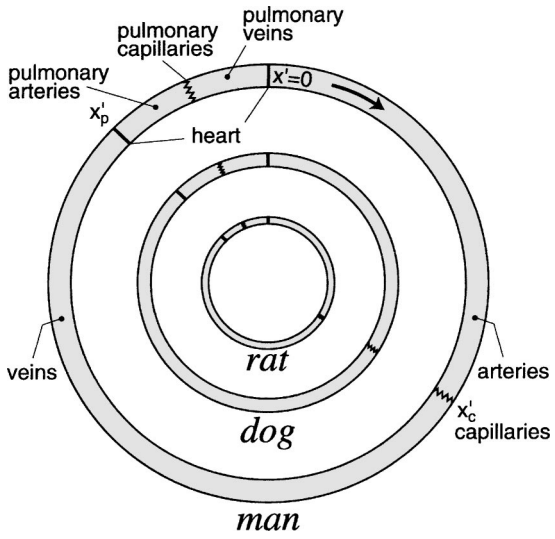


**FIGURE 2. Schematic representation of the ring shaped tube which models the circulatory system of a mammal. The blood flows clockwise. The tube of total length $L$, is divided into segments corresponding to the arterial, venular, pulmonary arterial, and pulmonary venular trees, respectively. The right site marked as heart ($x'=0$) corresponds to the left ventricle–left atrium, while the left site marked as heart ($x'=x'_p$) corresponds to the right ventricle–right atrium. Also, scaled down tubes are drawn corresponding to the circulatory systems of dog and rat; this provides a conceptual representation of the circulatory systems of the species for potential future applications.**

$$C(x',0)=c\exp\left(-\frac{b}{L^2}(x'-x'_{\text{inj}})^2\right), \quad (27)$$

where $c$ and $b$ are the shape parameters of the Gaussian. Actually, due to the special transformation, skewed initial condition would be more accurate than the symmetrical Gaussian, however, the fact that the Gaussian is considered ''thin'' makes it unimportant. Also, other types of intravenous administration, e.g., constant infusion, can be also considered. The center or the peak, $x'_{\text{inj}}$,

of the initial spatial profile for an intravenous bolus administration must be set at a high level of the tree structure, i.e., close to the heart (larger veins or arteries, two possible places). Similarly, when lung administration is considered, the peak of the initial condition should be set in the capillary area of the lungs ($x' = x'_p + (L - x'_p)/2$), Fig. 2. The total quantity $Q(t)$ inside the tube at any time $t$ is

$$Q(t) = \pi r_0^2 \int_0^L C(x',t)\,dx', \tag{28}$$

where $r_0$ is the radius of the tube, i.e., the radius of the aorta. From this relation, for $t=0$, an expression involving the blood volume $V_b = \pi r_0^2 L$, the initial dose, $Q(0)$, and the parameters of the initial condition, $c$ and $b$, can be derived assuming that $L$ is large,

$$Q(0) = c V_b \sqrt{\pi/b}. \tag{29}$$

Due to the geometrical character of the model, a sampling site, $x'_{\text{samp}}$, should be either specified, in simulation studies, or calculated when fitting is performed. Thus, a concentration versus time profile, $C(x'_{\text{samp},}t)$, can be obtained.

## VALIDATION OF THE MODEL

In order to verify the validity of our approach, the model is fitted to experimental human and dog data taken from literature.[18] The estimated values of the parameters are compared to physiological data.

The experimental concentration-time data for man correspond to a frequent sampling interval during the first 60 s after intravenous injection with 10 mg of indocyanine green (ICG), an intravascular tracer.[18] Both injection and sampling have been performed at relatively large vessels of the arm. Since ICG has significant hepatic uptake, even for such a short time, the contribution of uptake to the final profile is appreciable and is integrated in the model. A segment in the capillary region of the tube ($x' = x'_c$) is assigned as the uptake site and a first-order uptake term $-k_u C(x',t)$ is also considered in Eq. (22). The position of the uptake site is imprecise in physiological terms as it assumes blood flow through it to be equal to the heart output. Nevertheless, it is the most reasonable choice in order to keep the model simple. In fact, similar considerations have been made by Audi *et al.*[1] In future developments of the model, the positioning of organs that play important role in the disposition of substances can be implemented by adding parallel tubes at physiologically based sites to the present, simple, ring shaped model. The length of the uptake segment is arbitrarily set to $0.02\,L$, which is in the order of magnitude of the capillary length. We further introduce for convenience a new normalized coordinate $x^* = x'/L$, such that the total length of the tube is unity. Thus, the final model can be summarized mathematically as follows:

$$\frac{\partial C(x^*,t)}{\partial t} = \frac{\partial}{\partial x^*}\left( D^*(x^*)\frac{\partial C(x^*,t)}{\partial x^*}\right) - U_0^*\frac{\partial C(x^*,t)}{\partial x^*} - \Theta(x^*)k_u C(x^*,t), \tag{30}$$

where

$$D^*(x^*) = D_a^* \quad \text{for} \quad 0 < x^* \leqslant x_c^*,$$

$$D_a^*(x_p^* - x_c^*)/x_c^* \quad \text{for} \quad x_c^* < x^* \leqslant x_p^*,$$

$$D_p^* \quad \text{for} \quad x_p^* < x^* \leqslant 1,$$

and

$$\Theta(x^*) = 1 \quad \text{for} \quad x_c^* - 0.01 \leqslant x^* \leqslant x_c^* + 0.01,$$

and 0 otherwise,
where

$$D_a^* = D_a/L^2, \quad U_0^* = U_0/L.$$

Boundary and initial conditions are

$$C(0,t) = C(1,t), \quad D_a^*\left.\frac{\partial C}{\partial x^*}\right|_0 = D_p^*\left.\frac{\partial C}{\partial x^*}\right|_1$$

and

$$C(x^*,0) = Q(0)V_b^{-1}\sqrt{b/\pi}\exp[-b(x^* - x_{\text{inj}}^*)^2]. \tag{31}$$

Equation (30) was fitted to the ICG human data.[18] Parameters that are kept fixed in the model are: the length of the uptake site (0.02), the dose $Q(0) = 10$ mg, and the shape parameter $b = 10^5$ and the sampling point $x_{\text{samp}}^* = 0.02$. The injection point is considered relatively to the beginning of the pulmonary segment, namely, $x_{\text{inj}}^* = x_p^* - 0.02$, which roughly implements the experimental design, namely, i.v. bolus administration at the cephalic vein.[18] The parameter $n$ is considered to be equal to 3, because although the branching of the vascular tree is actually dichotomous,[2] its geometry is such that the number of vessels grows with each generation as if the tree was trichotomous.[13] So, $n=3$ has to be used in order to have the correct scaling laws.[32] All other parameters of the model including the coefficients $D_a^*$, $D_p^*$, $U_0^*$, the segment points $x_c^*$, $x_p^*$, the blood volume $V_b$, and the

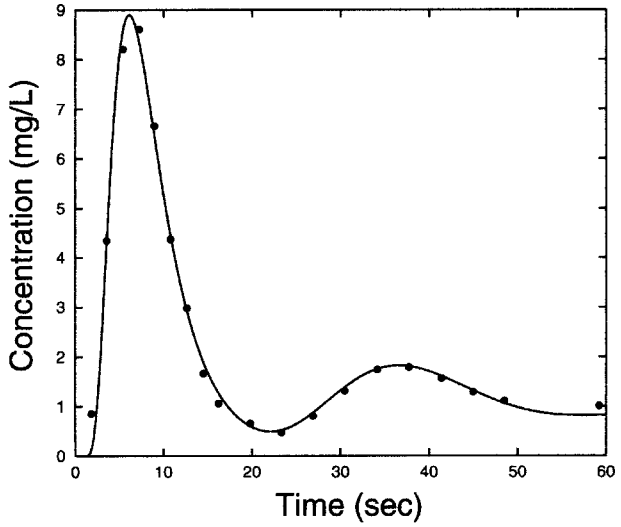


**FIGURE 3. Concentration-time plot of the experimental human data of ICG (Ref. 18) together with the fitted curve of the model. The two peaks correspond to respective passes of the center of the drug concentration distribution from the sampling site, as a result of recirculation.**

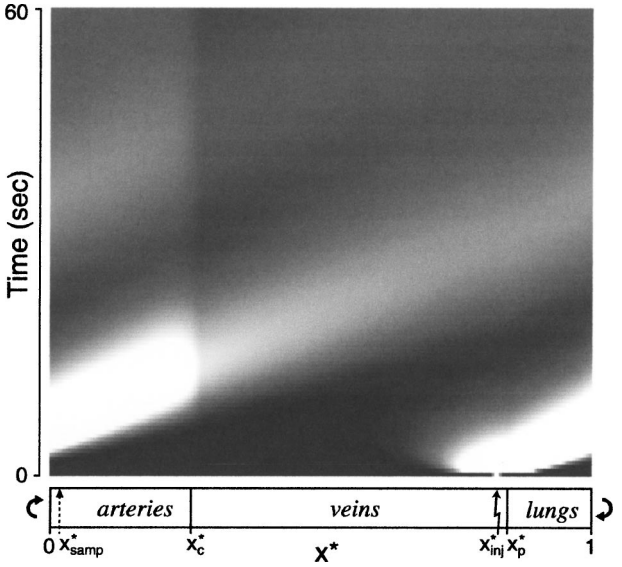


**FIGURE 4. Density plot of the temporal and spatial distribution of $C(x^*,t)$ for the human data of ICG in the normalized coordinate system. The two ends of the abscissa are connected. Light color stands for high concentration, dark stands for low. The parameters of the model for this simulation are listed in Table 1. The injection, sampling and the uptake sites for the simulated curve of Fig. 3 are also indicated.**

uptake rate constant $k_u$, are optimized by the fitting algorithm. The algorithm used is a classical Levenberg–Marquardt optimizer (LMDIF subroutine of the MINPACK Fortran optimization package; http://www.netlib.org/minpack/). The PDE is solved numerically using a Crank–Nicolson implicit finite-difference scheme.[25] As it is shown in Fig. 3. the accordance of the fitted curve with the data is satisfactory; the results of the optimization are shown in Table 1. Although the estimate for $V_b$ is reasonable,[18] the total blood volume may be underestimated because ICG distributes to both fast and slow compartments.[18] This has the result of underestimating the total blood volume as calculated from the first seconds because the portion of ICG following the slow route is not included in the calculation. Also, the transit time as depicted by the time distance of the two first peaks may not include these slow routes being underestimated as well. It has been shown that calculation of total blood volume based only on the first two peaks of ICG administration, without taking into account more complicated kinetics, underestimates blood volume up to 40%.[22] From the relation $V_b = \pi r_0^2 L$ and setting the value of the cross-sectional area of the aorta, $\pi r_0^2$, to be 3 cm$^2$,[10] a total tube length of $L = 1471$ cm is obtained. A density plot of the temporal and spatial distribution of the function $C(x^*,t)$ is presented in Fig. 4, where the sites $x^*_{\text{inj}}$ and $x^*_{\text{samp}}$ are indicated. The values for $x_c^*$ and $x_p^*$ are considered reasonable as well. The length of the pulmonary portion of the tube may be overestimated compared to the main

**TABLE 1. Estimates of the parameters derived from the fitting of Eq. (30) to experimental data of ICG from man[a] and dog.[b] Numbers in parentheses indicate the formal standard error as computed from the square root of the diagonal elements of the covariance matrix. Dashes indicate that the corresponding error could not be obtained with accuracy.**

| Parameter | Man | | Dog | |
|---|---|---|---|---|
| $x_c^*$ | 0.28 | (-) | 0.19 | (-) |
| $x_p^*$ | 0.85 | (0.0079) | 0.68 | (0.021) |
| $D_a^*$ (s$^{-1}$) | 0.000845 | (0.000031) | 0.00109 | (0.000018) |
| $D_p^*$ (s$^{-1}$) | 0.000470 | (-) | 0.000217 | (-) |
| $U_0^*$ (s$^{-1}$) | 0.0306 | (0.00096) | 0.0368 | (0.0013) |
| $k_u$ (s$^{-1}$) | 1.13 | (0.19) | 1.43 | (0.26) |
| $V_b$ (mL) | 4414 | (156.5) | 2228 | (98.8) |

[a]Reference 18.
[b]Reference 15.

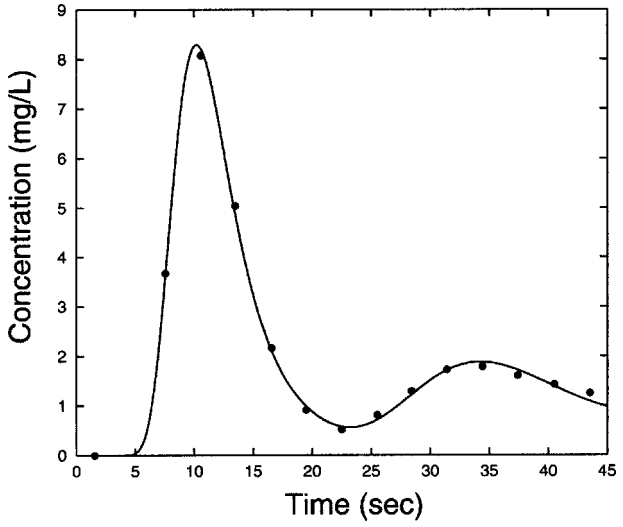


**FIGURE 5. Concentration-time plot of the experimental dog data of ICG (Ref. 15) together with the fitted curve of the model.**

circulation portion due to the already mentioned issue of the slow routes, as these exist only in the main circulation portion of the tube and are absent from the pulmonary portion. From Eqs. (23) we get an estimate for the velocity in the aorta

$$u_0 = U_0^* L - \frac{D_a^* L^2 \tilde{n}}{l_0}. \tag{32}$$

Using the estimated values of $D_a^*$, $U_0^*$, reported in Table 1 and $L = 1471$ cm and considering $l_0$ to be in the order of magnitude of the length of the aorta, $l_0 \approx 50$ cm, we can extract $u_0 \approx 34$ cm/s, which is a realistic value too.[10] The value of $D_a^* = 8.45 \times 10^{-4}$ s$^{-1}$, which corresponds to a geometrical dispersion coefficient $D_a = D_a^* L^2 = 1.8 \times 10^3$ cm$^2$/s justifies the argument of negligible molecular diffusion, where a typical value of the diffusion coefficient is of the order $10^{-5}$ cm$^2$/s. These results demonstrate that the model describes the data nicely (Fig. 3), while the estimates for the parameters are within the expected range.

In the same manner we analyzed dog data.[15] The experimental design is practically identical to the human study.[18] An intravenous injection 5 mg of ICG was followed by frequent blood sampling in the first 45 s. The results of the optimization are shown in Table 1. Figure 5 shows the plot of the experimental data together with the fitted curve. The same comments about the values of the fitted parameters apply as in the case of man. An interesting point however concerns the value of $x_p^*$ being rather small. Visual inspection of Fig. 5 reveals that the pulmonary transit time is comparable with the transit time of the main circulation, suggesting that dog has a higher ratio, pulmonary blood volume/main circulation blood volume, compared to man. However, this is probably due to the slow route kinetics issue, already mentioned, which seems to be attenuated in the case of the smaller mammals (dog). The presence of these slow routes also amplifies the dispersion of the main circulation portion compared to the pulmonary portion, a fact depicted at the calculated values of $D_a^*$ and $D_p^*$ in man and dog.

The analysis of ICG data in two species reveals that the model describes adequately the kinetics of ICG in both species. However, our data indicate that interspecies pharmacokinetic scaling,[4] related with the initial mixing of the tracers, should be considered with caution. This is so since the intravascular kinetics in various species do not manifest simple allometric laws, dependent exclusively on size. Instead, more detailed physiologically based description of kinetics is required. Our work is towards this quest. This notion is depicted in Fig. 2, showing the model developed, drawn schematically for various species.

## CONCLUSIONS

We derived a one-dimensional linear dispersion–convection equation with constant coefficients that describes the disposition of a substance inside a tree-like fractal network of tubes that emulates the vascular tree. Based on that result, a simple model for the mammalian circulatory system is built in entirely physiological terms consisting of a ring shaped, one-dimensional tube. The model takes into account dispersion, convection and uptake, describing the initial mixing of intravascular tracers. This model opens new perspectives in studies dealing with the disposition of intravascular tracers which are used for various hemodynamic purposes, e.g., cardiac output measurements,[18] volume of circulating blood determination[18] and liver function quantification.[11] Most importantly, the model can be expanded and used for the study of xenobiotics that distribute beyond the intravascular space. Consequently, applications can be envisaged in interspecies pharmacokinetic scaling and physiologically based pharmacokinetic-toxicokinetic modeling, since both fields require a realistic geometrical substrate for hydrodynamic considerations.

## APPENDIX

Derivation of Eq. (21):

If we substitute in Eq. (20),

$$\frac{\partial C(x',t)}{\partial t}=D(x)\left(\frac{\partial x'}{\partial x}\right)^2\frac{\partial^2 C(x',t)}{\partial x'^2}-\left(-\frac{\partial D(x)}{\partial x}\frac{\partial x'}{\partial x}-D(x)\frac{\partial^2 x'}{\partial x^2}+u(x)\frac{\partial x'}{\partial x}\right)\frac{\partial C(x',t)}{\partial x'} \quad (20)$$

the following expressions, for the various terms

$$D(x)=\left(a_1\sigma_{l0}+2\frac{a_2\sigma_{r0}l_0}{r_0}\right)\left(\frac{\pi r_0^2}{A(x)}\right)^2 u_0,$$

$$\frac{\partial D(x)}{\partial x}=2\frac{\pi r_0^2}{A(x)}\frac{1-n^{1/3}}{l_0 n^{1/3}}\left(a_1\sigma_{l0}+2\frac{a_2\sigma_{r0}l_0}{r_0}\right)u_0$$
$$=-2\frac{\pi r_0^2}{A(x)}\frac{\tilde{n}}{l_0}\left(a_1\sigma_{l0}+2\frac{a_2\sigma_{r0}l_0}{r_0}\right)u_0,$$

$$u(x)=\frac{\pi r_0^2}{A(x)}u_0,$$

$$\frac{\partial x'}{\partial x}=\frac{A(x)}{\pi r_0^2},$$

$$\frac{\partial^2 x'}{\partial x^2}=-\frac{1-n^{1/3}}{l_0 n^{1/3}}\left(\frac{A(x)}{\pi r_0^2}\right)^2=\frac{\tilde{n}}{l_0}\left(\frac{A(x)}{\pi r_0^2}\right)^2,$$

we end up with

$$\frac{\partial C(x',t)}{\partial t}=\left(a_1\sigma_{l0}+2\frac{a_2\sigma_{r0}l_0}{r_0}\right)u_0\left(\frac{\pi r_0^2}{A(x)}\right)^2\left(\frac{A(x)}{\pi r_0^2}\right)^2\times\frac{\partial^2 C(x',t)}{\partial x'^2}-\left\{2\frac{\pi r_0^2}{A(x)}\frac{\tilde{n}}{l_0}\left(a_1\sigma_{l0}+2\frac{a_2\sigma_{r0}l_0}{r_0}\right)u_0\frac{A(x)}{\pi r_0^2}-\left(a_1\sigma_{l0}+2\frac{a_2\sigma_{r0}l_0}{r_0}\right)\left(\frac{\pi r_0^2}{A(x)}\right)^2 u_0\frac{\tilde{n}}{l_0}\left(\frac{A(x)}{\pi r_0^2}\right)^2+\frac{\pi r_0^2}{A(x)}u_0\frac{A(x)}{\pi r_0^2}\right\}\frac{\partial C(x',t)}{\partial x'},$$

which finally simplifies to Eq. (21),

$$\frac{\partial C(x',t)}{\partial t}=\left(a_1\sigma_{l0}+2\frac{a_2\sigma_{r0}l_0}{r_0}\right)u_0\frac{\partial^2 C(x',t)}{\partial x'^2}-\left\{\frac{\tilde{n}}{l_0}\left(a_1\sigma_{l0}+2\frac{a_2\sigma_{r0}l_0}{r_0}\right)+1\right\}u_0\frac{\partial C(x',t)}{\partial x'}. \quad (21)$$

## ACKNOWLEDGMENT

This work was supported in part by the General Secretariat of Research and Technology of Greece. (EPAN-M.4.3 [2013555]).

## REFERENCES

[1] Audi, S. H., J. H. Linehan, G. S. Krenz, and C. A. Dawson. Accounting for the heterogeneity of capillary transit times in modeling multiple indicator dilution data. *Ann. Biomed. Eng.* 26:914–930, 1998.
[2] Bassingthwaighte, J. B., L. Liebovitch, and B. J. West. Fractal Physiol. Oxford: Oxford University Press, 1994.
[3] Beard, D., and J. B. Bassingthwaighte. Advection and diffusion of substances in biological tissues with complex vascular networks. *Ann. Biomed. Eng.* 28:253–268, 2000.
[4] Boxenbaum, H. Interspecies scaling, allometry, physiological time, and the ground plan of pharmacokinetics. *J. Pharmacokinet Biopharm.* 10:201–227, 1982.
[5] Brown, J. H., and G. B. West, eds. Scaling in Biology. Oxford: Oxford University Press, 2000.
[6] Edwards, D. A. A general theory of the macrotrasport of nondepositing particles in the lung by convective dispersion. *J. Aerosol Sci.* 25:543–565, 1994.
[7] Ellsworth, M. L., A. Liu, B. Dawamt, A. S. Popel, and R. N. Pittman. Analysis of vascular pattern and dimensions in arteriolar networks of the retractor muscle in young hamsters. *Microvasc. Res.* 34:168–183, 1987.
[8] Fung, Y. C. Biomechanics: Circulation. New York: Springer, 1997.
[9] Gerlowski, L. E., and R. K. Jain. Physiologically based pharmacokinetic modeling: principles and applications. *J. Pharm. Sci.* 72:1103–1127, 1983.
[10] Guyton, A. C., and J. E. Hall. Textbook of Medical Physiology. Philadelphia: Saunders, 2000.
[11] Hashimoto, M., and G. Watanabe. Simultaneous measurement of effective hepatic blood flow and systemic circulation. *Hepatogastroenterology* 47:1669–1674, 2000.
[12] Horsfield, K. Diameters, generations, and orders of branches in the bronchial tree. *J. Appl. Physiol.* 68:457–461, 1990.
[13] Huang, W., R. T. Yen, M. McLaurine, and G. Bledsoe. Morphometry of the human pulmonary vasculature. *J. Appl. Physiol.* 81:2123–2133, 1996.
[14] King, R. B., G. M. Raymond, and J. B. Bassingthwaighte. Modeling blood flow heterogeneity. *Ann. Biomed. Eng.* 24:352–372, 1996.
[15] Krejcie, T. C., M. J. Avram, W. B. Gentry, C. U. Niemann, M. P. Janowski, and T. K. Henthorn. A recirculatory model of the pulmonary uptake and pharmacokinetics of lidocaine based on analysis of arterial and mixed venous data from dogs. *J. Pharmacokinet Biopharm.* 25:169–190, 1997.
[16] LaBarbera, M. Principles of design of fluid transport systems in zoology. *Science* 249:992–1000, 1990.
[17] Lefevre, J. Teleonomical optimization of a fractal model of the pulmonary arterial bed. *J. Theor. Biol.* 102:225–248, 1983.
[18] Niemann, C. U., T. K. Henthorn, T. C. Krejcie, C. A. Shanks, C. Enders-Klein, and M. Avram. Indocyanine green kinetics characterize blood volume and flow distribution and their alteration by propranolol. *J. Clin. Pharm. Ther.* 67:342–350, 2000.
[19] Oliver, R. E., A. F. Jones, and M. Rowland. A whole-body

physiologically based pharmacokinetic model incorporating dispersion concepts: Short and long time characteristics. *J. Pharmacokinet Biopharm.* 28:27–55, 2001.

[20] Olufsen, M. S., C. S. Peskin, W. Y. Kim, E. M. Pedersen, A. Nadim, and J. Larsen. Numerical simulation and experimental validation of blood flow in arteries with structured-tree outflow conditions. *Ann. Biomed. Eng.* 28:1281–1299, 2000.

[21] Perl, W., and F. P. Chinard. A convection–diffusion model of indicator transport through an organ. *Circ. Res.* 12:273–298, 1968.

[22] Picker, O., G. Wietasch, T. W. Scheeren, and J. O. Arndt. Determination of total blood volume by indicator dilution: A comparison of mean transit time and mass conservation principle. *Intensive Care Med.* 27:767–774, 2001.

[23] Roberts, M. S., and M. Rowland. A dispersion model of hepatic elimination: 1. Formulation of the model and bolus considerations. *J. Pharmacokinet Biopharm.* 14:227–260, 1986.

[24] Scherer, P. W., L. H. Shendalman, and N. M. Greene. Simultaneous diffusion and convection in single breath lung washout. *Bull. Math. Biophys.* 34:393–412, 1972.

[25] Thomée, V. In: Handbook of Numerical Analysis, edited by Ciarlet, P. G., and J. L. Lions. Amsterdam: Elsevier, 1990, Vol. 1, pp. 5–195.

[26] Unice, K. M., and B. E. Logan. The insignificant role of hydrodynamic dispersion on bacterial transport. *J. Environ. Eng.* 126:491–500, 2000.

[27] van Beek, J. H., S. A. Roger, and J. B. Bassingthwaighte. Regional myocardial flow heterogeneity explained with fractal networks. *Am. J. Physiol.* 257:H1670–H1680, 1989.

[28] Vicini, P., R. C. Bonadonna, M. Lehtovirta, L. C. Groop, and C. Cobelli. Estimation of blood flow heterogeneity in human skeletal muscle using intravascular tracer data: Importance for modeling transcapillary exchange. *Ann. Biomed. Eng.* 26:764–774, 1998.

[29] Wagner, J. G. Pharmacokinetics for the Pharmaceutical Scientist. Lancaster, PA: Technomic, 1993.

[30] Weibel, E. R. Morphometry of the Human Lung. Berlin: Springer, 1963.

[31] Weiss, M., and W. Foster. Pharmacokinetic model based on circulatory transport. *Eur. J. Clin. Pharmacol.* 16:287–293, 1979.

[32] West, G. B., J. H. Brown, and B. J. Enquist. A general model for the origin of allometric scaling laws in biology. *Science* 276:122–126, 1997.

[33] West, G. B., J. H. Brown, and B. J. Enquist. The fourth dimension of life: Fractal geometry and allometric scaling of organisms. *Science* 284:1677–1679, 1999.

[34] Zamir, M., P. Sinclair, and T. H. Wonnacott. Relation between diameter and flow in major branches of the arch of the aorta. *J. Biomech.* 25:1303–1310, 1992.

[35] Zamir, M. On fractal properties of arterial trees. *J. Theor. Biol.* 197:517–526, 1999.